

Stability, Control, and Simulation of a Dual Lift System Using Autonomous R-MAX Helicopters

Marcos G. Berrios

Aerospace Engineer and PhD Candidate
Aviation Development Directorate-AFDD and Stanford University
US Army Research, Development and Engineering Command
Moffett Field, CA, USA

Mark B. Tischler

Senior Technologist and Flight Control Group Lead
Aviation Development Directorate-AFDD
US Army Research, Development and Engineering Command
Moffett Field, CA, USA

Luigi S. Cicolani

Aerospace Engineer
San Jose State University Research Foundation
Moffett Field, CA, USA

J. David Powell

Professor Emeritus
Department of Aeronautics and Astronautics
Stanford University, CA, USA

ABSTRACT

Cargo missions of the near future will require transportation of increasingly heavy loads to remote locations that are at distances farther, and at altitudes higher, than what can be accomplished by current helicopters. Using two helicopters to carry a single load, termed dual lift, provides heavy lift on demand and avoids the very costly design and development of a special purpose heavy lift helicopter. This paper discusses the stability and control aspects of a dual lift system using autonomous R-MAX helicopters. Unique dual lift modes lie in a frequency range that affect helicopter attitude responses and should be considered while designing an inner-loop (attitude) dual lift controller. One such mode is unstable and is characterized by the helicopters drifting away from each. In order to stabilize this mode, helicopter separation feedback is used. Unlike in a single lift system, there exists only one pendulum mode in a dual lift configuration and a cable angle that is relative to a no swing plane is needed to isolate the swinging motion and improve damping of the payload. With the identified control challenges as a foundation, a multi-objective parametric optimization approach is used to design a controller for a dual lift system that meets a comprehensive set of ADS-33E stability and performance specifications.

NOTATION

${}^N \vec{a}^{B1_{cm}}$	Acceleration of point $B1_{cm}$ in reference frame N , $\frac{ft}{sec^2}$
$\underline{I}^{B1_{cm}}$	Inertia dyadic of $B1$ about $B1_{cm}$, $slug-ft^2$
$I_{b1_x, b1_x}$	Roll moment of inertia of $B1$ about $B1_{cm}$, $slug-ft^2$
$I_{b1_y, b1_y}$	Pitch moment of inertia of $B1$ about $B1_{cm}$, $slug-ft^2$

$I_{b1_z, b1_z}$	Yaw moment of inertia of $B1$ about $B1_{cm}$, $slug-ft^2$
$\vec{r}^{B1_{cm}}_{N_o}$	Position vector from point N_o to $B1_{cm}$, ft
${}^N \vec{v}^{B1_{cm}}$	Velocity of point $B1_{cm}$ in reference frame N , $\frac{ft}{sec}$
${}^N \ddot{\alpha}^{B1}$	The angular acceleration of $B1$ in N , $\frac{rad}{sec^2}$
${}^N \vec{\omega}^{B1}$	The angular velocity of $B1$ in N , $\frac{rad}{sec}$
ADS	Aeronautical Design Standard
AFCS	Automatic Flight Control System
AFDD	Aeroflightdynamics Directorate
ARP	Autonomous Rotorcraft Project
DOF	Degree of Freedom
DRB	Disturbance Rejection Bandwidth, $\frac{rad}{sec}$
DRP	Disturbance Rejection Peak, dB
FBD	Free Body Diagram

Presented at the AHS 70th Annual Forum, Montréal, Québec, Canada, May 20–22, 2014. This is a work of the U.S. Government and is not subject to copyright protection in the U.S. DISTRIBUTION STATEMENT A. Approved for public release; distribution is unlimited.

<i>FCS</i>	Flight Control System
<i>LMR</i>	Load Mass Ratio
<i>PPF</i>	Pendant Penalty Fraction

INTRODUCTION

Helicopters play a vital role in moving cargo from point to point. Whether the application is industrial, military, or humanitarian, there is often no other practical way to deliver material or equipment to remote locations. Cargo missions of the near future will require transportation of increasingly heavy loads to remote locations that are at distances farther, and at altitudes higher, than what can be accomplished by current helicopters. One solution is to build larger aircraft, but this approach works only to a point. A practical size limit is quickly reached when evaluating the return-on-investment of designing, building, and operating a specialized heavy-lift vehicle (Ref. 1). Using two helicopters to carry a single load, termed “dual lift”, provides heavy lift on demand and avoids the very costly design and development of a special purpose heavy lift helicopter.

The concept of a two or more lift system termed “multi-lift” has been studied extensively in the past. Early studies looked at the feasibility of various configurations (Ref. 2), followed by very limited manned flight testing (Ref. 3), and concluded that a system could work if increased levels of control augmentation or autonomy were present (Ref. 4). As a result, many simplified (Refs. 5, 6) and complex (Refs. 7, 8) simulation models were developed and used to design flight control systems for multi-lift systems. These control systems range from simple classical feedback architectures (Refs. 6, 9) to more sophisticated nonlinear feedback techniques (Refs. 10, 11, 12). Recently, there has been a limited flight demonstration of a control system applied to a multi-lift configuration using three small sized helicopters (Ref. 13).

The dual lift research effort at the US Army Aviation Development Directorate (AFDD) and Stanford University is to develop and flight test a complete control system that is representative of, and can be confidently scaled for, a full sized system. This controller is being applied to a medium sized dual lift system using autonomous R-MAX helicopters (Figure 1). R-MAX helicopters have been successfully used as a developmental research platform prior to testing technology on a full sized aircraft (Ref. 14), such as a UH-60 Black Hawk.

The dual lift controller will accept, as its input, waypoints that the dual lift system will need to track. As an example, an obstacle field navigation routine, as in Reference 15, can define a desired trajectory of the load for the dual lift control system. The controller will then maneuver the helicopters so that the load follows the given trajectory while maintaining stability and minimizing an objective function consisting of parameters such as total thrust, fuel consumption, and load distribution. As a starting point, the dual lift controller builds upon an existing control architecture developed by the Autonomous Rotorcraft Project (ARP) at Moffett Field, CA for a single R-MAX helicopter (Ref. 16). The inner-loop of the existing controller will be augmented to stabilize and increase

robustness of the system by accounting for the dual lift dynamics. A new outer-loop will then be developed that optimally maneuvers the helicopters to track a given trajectory.

This paper focuses on gaining a fundamental understanding of the dynamic behavior of a dual lift system and the associated flight control challenges. To do so, a dual lift simulation model using two R-MAX helicopters is developed and verified. Upon verification of the simulation model, the unique stability characteristics of the dual lift system are studied and flight control strategies are developed. An existing inner-loop controller developed by ARP for a single R-MAX is then augmented with unique dual lift measurements to meet a comprehensive set of stability and performance specifications.



Fig. 1. Autonomous R-MAX helicopters flown by the Autonomous Rotorcraft Project (ARP) at Moffett Field, CA

SYSTEM DESCRIPTION

In 1957, the Vertical Aircraft Corporation (Vertol) conducted a feasibility study for multiple multi-lift helicopter system configurations (Ref. 2). The two concepts that were most practical used two helicopters and were termed “spreader bar” and “pendant” configurations (Fig. 2). The earlier study found the pendant system to be the simplest, lightest configuration and easiest to assemble. Due to its minimalistic makeup, the system also exhibits the least amount of drag and, as a result, has better long range capabilities. The disadvantages of the pendant configuration include unusual trim attitudes, no positive separation of the helicopters, and long cables. Because the concept of dual lift was originally intended to be pursued in a manned capacity, the noted disadvantage of unusual trim attitudes were unacceptable for pilots and rendered the pendant configuration impractical and the spreader bar configuration was chosen. In the near future, however, the typical cargo mission may be autonomous in nature (Ref. 17). With an unmanned application in mind, the mentioned disadvantage of unusual trim attitudes is no longer applicable and the pendant configuration becomes a very attractive solution and is the configuration studied in this research effort.

System Geometry

Figure 3 shows a model of a pendant dual lift system consisting of two helicopters, $B1$ and $B2$, separated by a distance h_s and with formation angle of ψ_f . Massless cable C_i (for

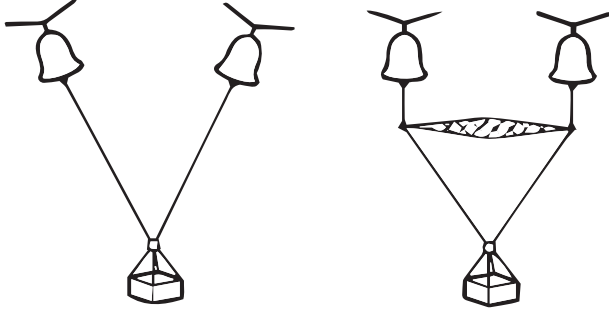


Fig. 2. Pendant (left) and spreader bar (right) dual lift configurations. (Ref. 18)

$i = 1, 2$) is connected with a frictionless ball joint to helicopter Bi at the hook attachment point Bi_{hk} and to the payload L at the payload sling attachment connection point L_{hk} .

Unit vectors $\hat{b}i_j$ and \hat{l}_j (for $j = x, y, z$) are standard body axes fixed in Bi and L with $\hat{b}i_z$ and \hat{l}_z pointing downward. Cable axes $\hat{c}i_j$ are fixed in Ci with $\hat{c}i_z$ pointing downward. N is taken to be a local North-East-Down (NED) inertial frame with origin at point N_o and \hat{n}_z pointing downward. All unit vectors are right-handed and orthogonal.

The orientations of Bi and L , with respect to N , are characterized by euler angles via a Body321 rotation sequence $(\psi_i, \theta_i, \phi_i)$ and $(\psi_L, \theta_L, \phi_L)$, respectively. The cable frame Ci is a local vertical, local horizontal frame aligned with the heading of Bi . Its orientation is obtained via a Body321 sequence $(\psi_i, \theta_{ci}, \phi_{ci})$, also with respect to N . Relevant identifiers for the dual lift pendant system are listed in Table 1.

Table 1. List of relevant dual lift configuration parameters

Quantity	Symbol
Inertial North-East-Down frame	N
Helicopter i and body-fixed frame	Bi
Load body-fixed frame	L
Cable i frame	Ci
Inertial coordinates of Bi and L	$(x_i, y_i, z_i), (x_L, y_L, z_L)$
Euler angles of Bi and L w.r.t. frame N	$(\phi_i, \theta_i, \psi_i), (\phi_L, \theta_L, \psi_L)$
Euler angles of Ci w.r.t. frame N	$(\psi_i, \phi_{ci}, \theta_{ci})$
Mass of Bi , and L	m^{Bi}, m^L
Inertia dyadic of Bi about Bi_{cm}	$I^{Bi}_{Bi_{cm}}$
Length of cable Ci	l_{c_i}
Distance from Bi_{cm} to Bi_{hk}	h_i
Distance from L_{hk} to L_{cm}	h_l
Distance from $B1_{cm}$ to $B2_{cm}$	h_s
Formation angle	ψ_f

STATIC TRIM ANALYSIS

In a pendant configuration the load hangs underneath both helicopters, forming a shape similar to that of a pendant hanging

from one's neck. The lack of a spreader bar imposes a non-zero trim attitude in hover. This non-zero attitude tilts each helicopter's thrust vector away from the vertical axis, creating a horizontal component of thrust that is used to maintain helicopter separation and not to carry the load. Therefore, this horizontal thrust component is a direct measure of penalty for the pendant configuration. A static force analysis can be used to choose practical values for configuration parameters, such as cable length and helicopter separation, that result in acceptable lifting capabilities; ultimately, defining a nominal configuration.

A pendant penalty fraction (PPF) for each helicopter can be defined as the ratio of the helicopter's non-vertical thrust to the percentage of the load weight the helicopter is required to lift. Such an expression takes the form,

$$PPF(\%) \triangleq \frac{\|\vec{T} - \vec{T} \cdot \hat{n}_z\|}{\beta W_L} \times 100 \quad (1)$$

where \vec{T} is the trim helicopter thrust vector in hover, β the load sharing fraction, and W_L is the weight of the load. A static trim analysis of the pendant configuration was conducted under the assumptions of equal load sharing, $\beta = \frac{1}{2}$, identical helicopters, and that all forces are applied at each bodies respective center of gravity. The latter assumption allows the analysis to be purely a force balance problem and the results to be helicopter independent.

The PPF was calculated as a function of cable length and helicopter separation for various load mass ratios (LMR),

$$LMR_i \triangleq \frac{\beta \cdot m^L}{m^{Bi} + \beta \cdot m^L} \quad (2)$$

with typical values of LMR ranging from 0.1 - 0.3 for a single lift system. Given a nominal helicopter separation, h_s , of two rotor diameters (c.g.-to-c.g.), Figure 4 shows the PPF as a function of cable length. Increasing cable length decreases the penalty fraction, thereby increasing the lifting efficiency of the system. The exponential-like decay of the PPF indicates that a large reduction in penalty is achieved for a cable length of two and a half rotor diameters while minimal gains in efficiency are seen past three rotor diameters. Ideally, one would choose a configuration with as long a cable as possible, however, that desire must be tempered by practicality. A K-MAX helicopter uses a sling length of 0.63 to 2.1 rotor diameters (30-100 ft), suggesting that a cable length of two rotor diameters is a good compromise between performance and functionality.

Figure 5 shows the PPF as a function of helicopter separation for various values of LMR. Increasing helicopter separation increases the penalty fraction, thereby decreasing the lifting efficiency of the system. A large and rapid increase in penalty is observed for a helicopter separation greater than two rotor diameters. In close formation flight of manned helicopters, separation distances of two to four rotor diameters are typical. For a UH-60, this corresponds to a distance of

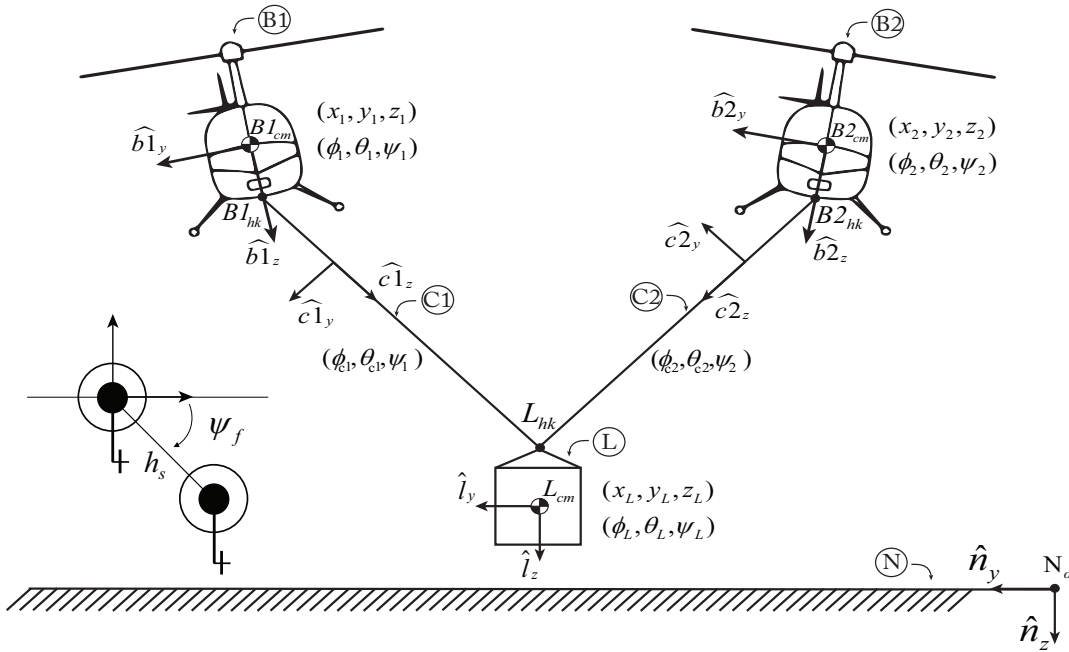


Fig. 3. System geometry for dual lift pendant configuration.

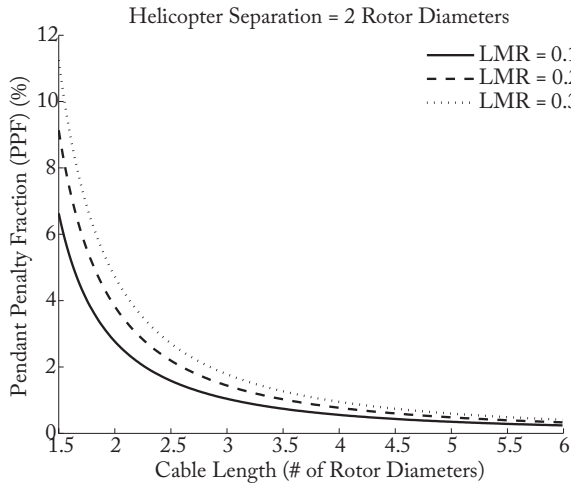


Fig. 4. Pendant penalty fraction as a function of cable length for various values of load mass ratio

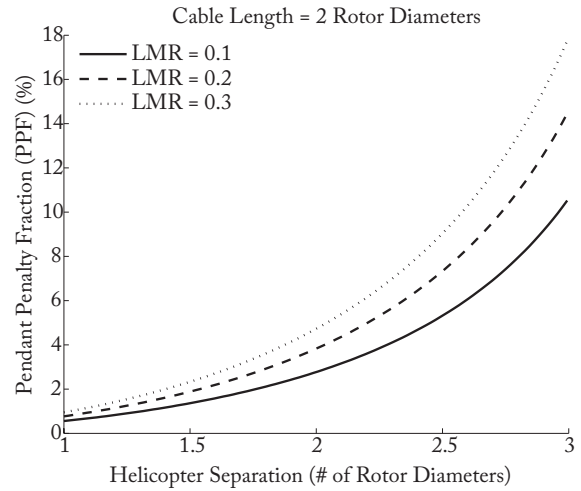


Fig. 5. Pendant penalty fraction as a function of helicopter separation for various values of load mass ratio

approximately 100 to 200 feet. Therefore, a separation of two rotor diameters serves as a good balance between safety and performance.

Choosing a cable length and helicopter separation of two rotor diameters yields, approximately, a 5% penalty fraction. Equivalently, this means that a dual lift pendant system can achieve a 95% increase in maximum lifting capability with cable length and helicopter separation of two rotor diameters when compared to a single lift system. Therefore, a cable length and helicopter separation of two rotor diameters is practical and provides good performance, defining the

nominal configuration studied in this paper.

EQUATIONS OF MOTION

The nonlinear equations of motion for the dual lift pendant configuration were derived using the Newton-Euler method in the symbolic dynamics environment, MotionGenesisTM Kane (Ref. 19). Each R-MAX helicopter is modeled as a rigid body and its aerodynamics represented by stability and control derivatives identified in flight by Cheng, et al. (Ref. 20) for a hover condition. In addition to the rigid body states,

the flight identified R-MAX dynamics include coupled rotor/fuselage, rotor/stabilizer, and heave/coning/inflow dynamics. The cables connecting the helicopters to the load are considered massless and can be elastic or inelastic. The load can be modeled as a point mass or rigid body if the aerodynamic characteristics are known.

Applying the Newton-Euler method to the free body diagram (FBD) of B1 (Fig. 6) yields

$$\vec{F}_{Aero}^{B1} + \vec{F}_T^{B1} + \vec{F}_g^{B1} = m^{B1} * {}^N \vec{a}^{B1_{cm}} \quad (3)$$

$$\begin{aligned} \vec{M}_{Aero}^{B1} + \vec{r}^{B1_{hk}} \times \vec{F}_T^{B1} &= \underline{I}^{B1_{cm}} \cdot {}^N \vec{\alpha}^{B1} \\ &+ {}^N \vec{\omega}^{B1} \times (\underline{I}^{B1_{cm}} \cdot {}^N \vec{\omega}^{B1}) \end{aligned} \quad (4)$$

where \vec{F}_{Aero}^{B1} is the helicopter aerodynamic and control force, \vec{F}_T^{B1} is the cable tension, \vec{F}_g^{B1} is the gravitational force, and \vec{M}_{Aero}^{B1} is the aerodynamic and control moment. Similarly, the Newton-Euler equations for B2 and L (Fig. 7) are

$$\vec{F}_{Aero}^{B2} + \vec{F}_T^{B2} + \vec{F}_g^{B2} = m^{B2} * {}^N \vec{a}^{B2_{cm}} \quad (5)$$

$$\begin{aligned} \vec{M}_{Aero}^{B2} + \vec{r}^{B2_{hk}} \times \vec{F}_T^{B2} &= \underline{I}^{B2_{cm}} \cdot {}^N \vec{\alpha}^{B2} \\ &+ {}^N \vec{\omega}^{B2} \times (\underline{I}^{B2_{cm}} \cdot {}^N \vec{\omega}^{B2}) \end{aligned} \quad (6)$$

and

$$\vec{F}_{Aero}^L + \vec{F}_g^L - \vec{F}_T^{B1} - \vec{F}_T^{B2} = m^L * {}^N \vec{a}^{L_{cm}} \quad (7)$$

$$\begin{aligned} \vec{M}_{Aero}^L - \vec{r}^{L_{hk}} \times (\vec{F}_T^{B1} + \vec{F}_T^{B2}) &= \underline{I}^{L_{cm}} \cdot {}^N \vec{\alpha}^L \\ &+ {}^N \vec{\omega}^L \times (\underline{I}^{L_{cm}} \cdot {}^N \vec{\omega}^L). \end{aligned} \quad (8)$$

This study focuses on hover and low speed flight where the aerodynamics of the payload is not significant. Therefore, the payload is modeled as a point mass by neglecting its aerodynamics and setting the payload c.g.-to-sling attachment distance to zero, $\vec{r}^{L_{hk}} = 0$. In addition, the cables are considered massless and inelastic. Given the inelastic assumption, two kinematic constraint equations that represent the invariance of the cable lengths are needed. Namely,

$$f_i = \|\vec{r}^{L_{hk}}\| - l_{c_i} = 0, \quad i = 1, 2 \quad (9)$$

where l_{c_i} is the length of cable i . In order to enforce this nonlinear configuration constraint during numerical simulation without solving a nonlinear algebraic equation at each time step, a constraint stabilization technique is used as described by Mitiguy in Reference 19. A motion constraint equation ($\dot{f}_i = 0$) and agitation constraint equation ($\ddot{f}_i = 0$) are formed and combined to produce a new pseudo-holonomic constraint as follows:

$$\ddot{f}_i + k_d \dot{f}_i + k_p f_i = 0, \quad i = 1, 2 \quad (10)$$

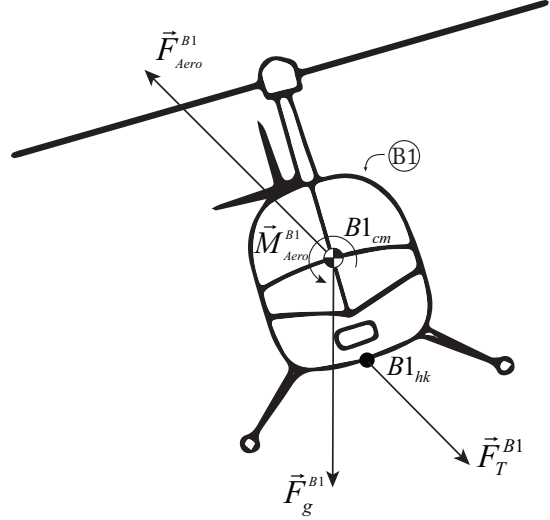


Fig. 6. Free body diagram of B1

The constants k_d and k_p define the rate at which $f_i(t)$ decays to zero.

Together, the three sets of Newton-Euler equations (3 - 8) and the two kinematic constraint equations (10) form the complete set of nonlinear differential equations for the dual lift pendant configuration.

Model Verification

It is important to check the accuracy of a completed dynamic simulation. Inadequate accuracy can arise if a mistake is made in the formulation of the equations of motion, if the equations are coded incorrectly despite correct formulation, or if the numerical integration routine itself is imperfect (Ref. 21). One common method for testing the simulation models of mechanical systems is to use conservation principles, such as the conservation of mechanical energy. However, conservation principles for models that include aerodynamic forces do not hold because the forces are dissipative in nature; for example, drag.

Therefore, a dissipative energy integral developed by Kane, Levinson, and Mitiguy (Ref. 21, 19), that is always constant and deals with systems involving energy dissipation, is used to test the numerical accuracy of the dual lift model. The energy integral is defined to be

$$E_Z \triangleq K_2 + V + Z \quad (11)$$

where E_Z is a constant with units of energy, K_2 is the system kinetic energy of degree 2, V is the systems generalized potential energy, and Z is a differential equation that is a function of the non-conservative generalized power of the system. The soundness of the dual lift dynamics was verified by formulating the dissipative energy integral and tracking its value throughout a numerical simulation. In this simulation, two consecutive doublets were applied to each helicopter control axis simultaneously. The energy integral remained within $-2 \times 10^{-4} ft - lb$ of it's original value of zero when using an

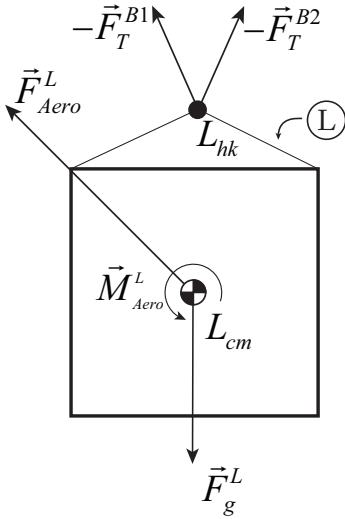


Fig. 7. Free body diagram of payload, L

8th order ODE solver with a step size of 1 ms (Fig. 8). An energy of $-2 \times 10^{-4}\text{ ft-lb}$ is equivalent to the kinetic energy of a R-MAX with a velocity of 0.009 ft/s , well within reasonable losses.

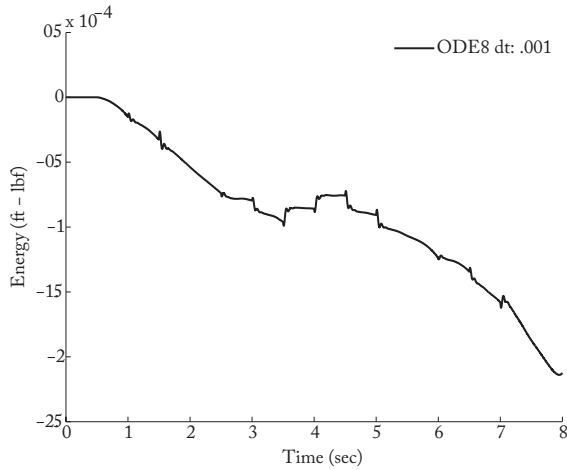


Fig. 8. Energy dissipated throughout a sample numerical simulation in which two consecutive doublets were applied to each helicopter control axis simultaneously

A second model verification process involved “collapsing” the dual lift dynamics to that of a single R-MAX with slung load and comparing to an already existing single lift model of an R-MAX that was developed independently by Cicolani (Ref 22). Figure 9 overlays the low frequency system poles for both single lift models. Excellent agreement is observed with essentially perfect matches of both pendulum modes and single unstable phugoid. The high frequency modes associated with the coupled rotor/stabilizer/fuselage dynamics also shows excellent agreement.

Favorable results from the two verification processes leads to a high degree of confidence in the formulation of the dual lift dynamics, forming a foundation for modal analysis and control law development.

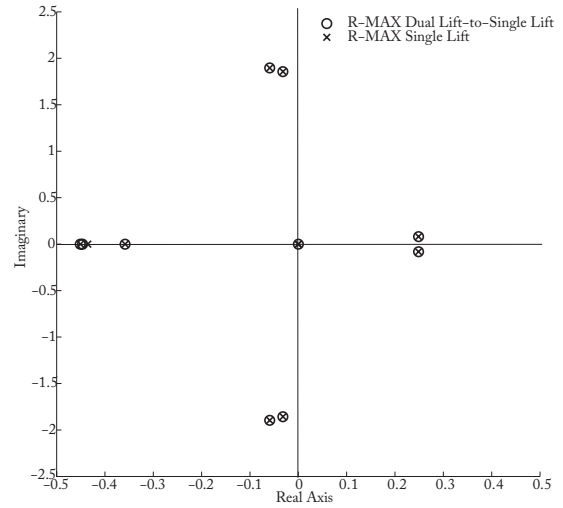


Fig. 9. Low frequency pole-zero map comparison of two independently developed models of a single R-MAX with slung load

MODAL ANALYSIS

A modal analysis of the dual lift pendant configuration provides fundamental insight of the intrinsic behavior of the system and exposes potential difficulties in control law development. The analysis considers the bare-airframe dynamics of the two R-MAXs and does not include any control system augmentation. Table 2 summarizes the nominal configuration parameters used in the analysis. Cable lengths and a helicopter separation of two rotor diameters (20.5 ft) with a LMR of 0.25 are used. In addition, a nominal formation angle (Fig. 3) of 45 deg is chosen to study the lateral and longitudinal coupling of the aircraft and load motion.

For a dual lift pendant configuration, there exists five unique multi-body modes not present in a single lift system (Fig. 10). Of the five multi-body modes, one is unstable and is characterized by both helicopters drifting away from each other with a time to double amplitude of 1.64 seconds. This “helicopter divergence” mode exists because the cable-hook attachment point is below each helicopter’s center of gravity (c.g.). In trim, there exists a non-vertical hook force that generates a moment about each helicopter’s c.g. and, when perturbed, causes the helicopters to drift apart. This mode is consistent with findings in References 6, 9, and 23 for a planar, 3-DOF spreader bar configuration. Because of the planar assumption in the cited references, the helicopter formation angles were either $\psi_f = 0$ (side-by-side) or $\psi_f = 90$ (front-to-back) and restricted the helicopter separation to be purely

Table 2. Nominal dual lift hover configuration parameters

Symbol	Value
(x_1, y_1, z_1)	$(0, 0, -100)$ [ft]
(x_2, y_2, z_2)	$(-14.5, 14.5, -100)$ [ft]
m^{B1}, m^{B2}	4.97 [slugs]
m^L	3.30 [slugs]
LMR	0.25 [-]
$I_{b1_x b1_x}, I_{b2_x b2_x}$	2.7 [slug-ft ²]
$I_{b1_y b1_y}, I_{b2_y b2_y}$	10.3 [slug-ft ²]
$I_{b1_z b1_z}, I_{b2_z b2_z}$	9.05 [slug-ft ²]
lc_1, lc_2	20.5 [ft]
h_1, h_2	1.5 [ft]
h_l	0 [ft]
h_s	20.5 [ft]
ψ_f	45 [degs]

lateral or longitudinal. From these results, one could hypothesize that the formation angle determines the direction in which the helicopters diverge. However, it was found that the individual helicopter's unstable phugoid played a major role in determining the direction of divergence, not formation angle.

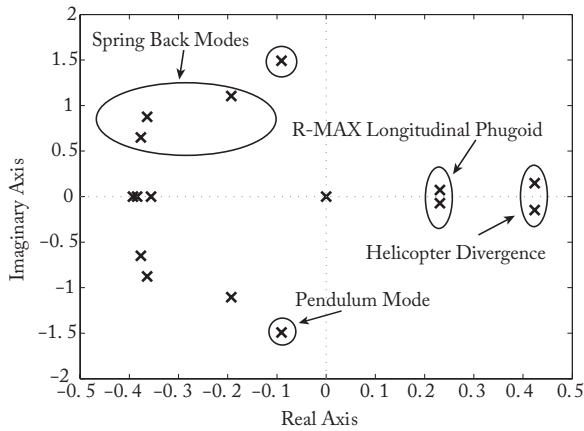


Fig. 10. Low frequency system roots of a dual lift pendant configuration showing the R-MAX's unstable phugoid and new multi-body modes not present in a single lift system

Figure 11 shows a phasor diagram of the helicopter divergence mode for various formation angles. To generate the diagram, the eigenvector associated with the divergent mode was scaled such that $1deg = 1 \frac{deg}{s} = 1ft = 1 \frac{ft}{s}$, then the eigenvector was normalized, and finally the six most influential states were plotted. The branches of the phasor diagram associated with the longitudinal positions of both helicopters (x_1 and x_2) have a magnitude of 1 for all formation angles, clearly indicating that the helicopter divergence mode is dominated by longitudinal separation and is independent of formation angle.

This behavior can be attributed to the fact that the R-MAX's unstable phugoid is dominated by longitudinal states such as pitch angle and longitudinal body velocity. As suggested by Curtiss and Hess for a 3-DOF spreader bar configuration, this unstable mode could potentially be stabilized by having helicopter separation information available and incorporating this measurement into the feedback loop.

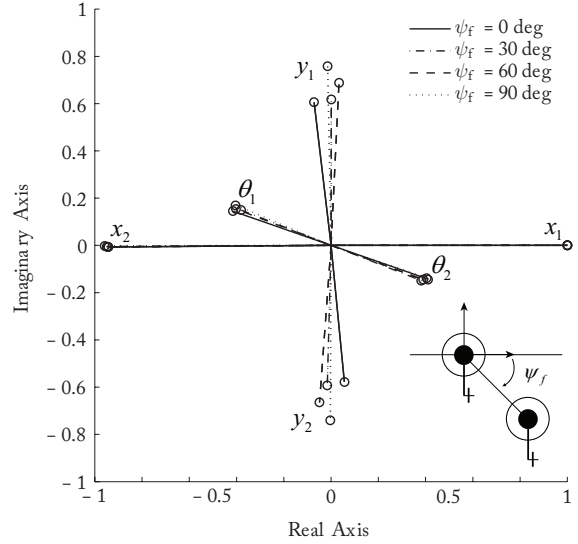


Fig. 11. Phasor diagram of helicopter divergence mode for various formation angles

In Reference 24, Raz studied the dynamic modes of a 6-DOF dual lift spreader bar configuration. The helicopters were at a fixed formation angle of 45 deg and each helicopter's automatic flight control system (AFCS) was engaged. The system's equivalent divergent mode was characterized by lateral separation of the helicopters and yaw oscillations of the spreader bar. It was also found that this divergent mode was significantly affected by the helicopter's AFCS, suggesting that the direction of separation was ultimately determined by the individual helicopter's characteristics with an engaged AFCS.

In addition to the helicopter divergent mode, there are three spring back modes; one associated with each axis (lateral, longitudinal, and, vertical). These modes are characterized by the helicopters moving towards and away from each other as if connected by a spring and damper. Figures 12 and 13 show a visual depiction of the described behavior for the lateral and vertical axis, respectively. Table 3 summarizes the frequency and damping characteristics of the three spring back modes. Note that the frequency of each mode is within a factor of 3 of a nominal attitude broken-loop crossover of $2 \frac{rad}{sec}$, indicating that these modes will influence the design of an inner loop controller.

One major difference between a single and dual lift system is the presence of only one pendulum mode for the dual lift configuration. Introducing an additional helicopter and at-

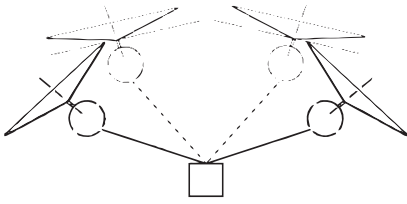


Fig. 12. Lateral spring back motion for a pendant dual lift configuration

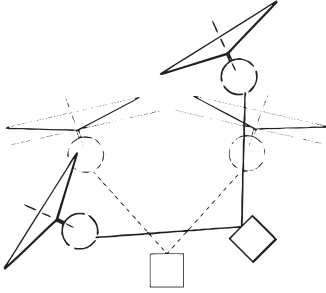


Fig. 13. Vertical spring back motion for a pendant dual lift configuration

tachment point for the payload eliminates one of the load's degrees of freedom under the assumption of taut cables. The swinging motion of the load is constrained to move perpendicular to a "no swing" plane formed by the hook attachment points of each helicopter and the downward pointing inertial axis as shown in Figure 14. The frequency of the pendulum mode for a pendant system can be estimated by the simple relation of a 1-DOF pendulum,

$$\omega_{pend} = \sqrt{\frac{g}{l}} \quad (12)$$

where the effective cable length (l) is the height of the load below the helicopters. Because this height is smaller than the original cable length, the natural frequency of the dual lift pendulum mode is slightly larger than that of a single lift system.

CONTROL LAW DEVELOPMENT

This research takes a first look at addressing the flight control challenges of a pendant dual lift system by designing an inner-loop (attitude) controller that meets aeronautical design standard performance specifications ADS-33E-PRF (Ref. 25). Such a controller will serve as a foundation for a future design of a dual lift outer-loop/trajjectory following control system.

The flight control system (FCS) designed by the Autonomous Rotorcraft Project (ARP) at Moffett Field, CA for a single R-MAX helicopter is described in Reference 16 and depicted in Figure 15. The FCS accepts raw waypoints, generates a feasible path, and tracks a commanded position and heading. Because this study focuses on designing a dual lift inner-loop (attitude) controller, only the inner-loop of the R-MAX's FCS is considered.

Table 3. Unique dynamic modes present in a dual lift pendant configuration with no control system

Mode Description	Eigenvalue	Frequency $\frac{rad}{sec}$	Damping
Helicopter Divergence	$0.41 \pm 0.15i$	0.45	-0.94
Lateral Spring Back	$-0.38 \pm 0.65i$	0.75	0.50
Longitudinal Spring Back	$-0.36 \pm 0.88i$	0.95	0.38
Vertical Spring Back	$-0.19 \pm 1.1i$	1.1	0.17
Pendulum Mode	$-0.09 \pm 1.5i$	1.5	0.06

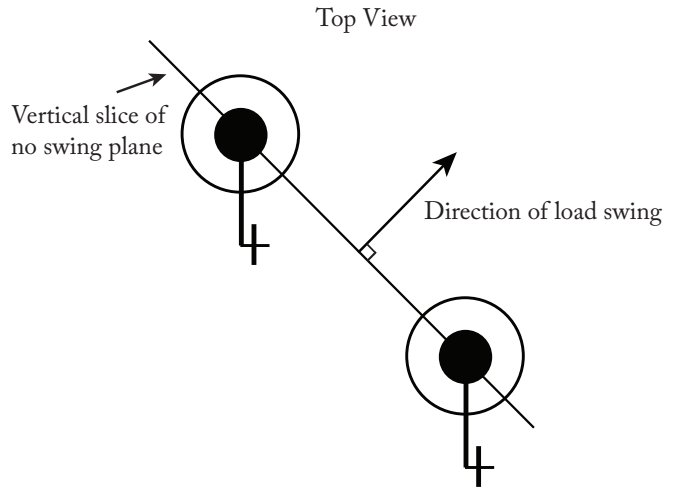


Fig. 14. Top view of a pendant dual lift configuration showing the direction of load swinging

Figure 16 shows the current roll axis inner-loop architecture being flown on the R-MAX by ARP with the other axes following the same structure. The control architecture consists of an attitude command-attitude hold (ACAH) response type and is a variation on a classic explicit model following system. In a classical explicit model following controller, the inverse of the bare-airframe model is used in the feed forward path. Instead, as shown in Figure 16, the inverse of the closed loop response, $P(s)$, is used as a pre-filter to cancel the dynamics of the feedback loop and track the desired command model. In turn, the dynamics of the feedback loop determine the stability and disturbance rejection properties of the system.

The dual lift controller developed herein builds upon and augments the existing ARP inner-loop control architecture as shown in Figure 17. The dual lift augmentation block (in gray) calculates an additional set of actuator commands that supplements the commands from the existing ARP inner-loop. This approach would allow for a similar dual lift controller to be applied to an existing autonomous aircraft such as a K-MAX (Ref. 17) or UH-60 (Ref. 14).

Baseline Performance

Even though the current control system flown on the R-MAX was not designed with a dual lift system in mind, it still serves

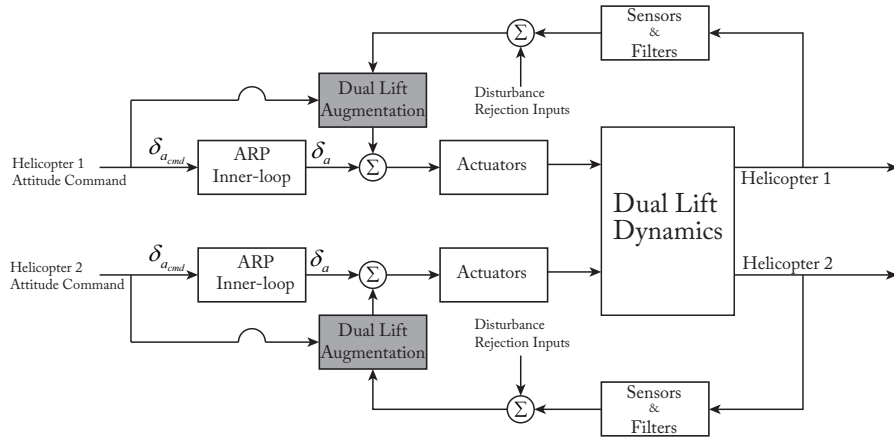


Fig. 17. Top level block diagram of dual lift controller with augmented inner-loop shown in gray

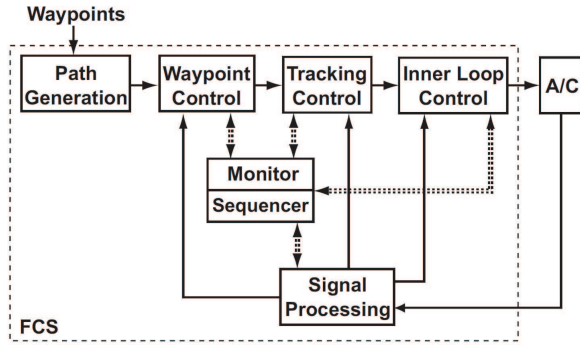


Fig. 15. Top level FCS block diagram for a single R-MAX (Ref. 16)

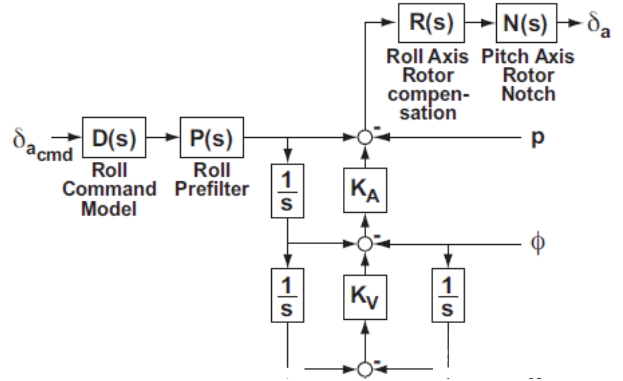


Fig. 16. ARP roll inner-loop controller (Ref. 16)

as a baseline controller that assesses the behavior of a dual lift system with no additional augmentation. Therefore, the performance of a dual lift system in which each R-MAX only uses ARP's current inner-loop controller is assessed in the Simulink[®] environment.

Figure 18 shows the low frequency roots for a dual lift system with the baseline controller. The dual lift system is still unstable, though much less than the bare-airframe system of Figure 10. As compared to the unaugmented system, the helicopter divergent mode has a larger frequency of $0.8 \frac{rad}{sec}$ and a much larger time to double amplitude of 41.2 seconds. The frequency of the lateral spring back mode differs only slightly, but the damping ratio was significantly reduced from 0.50 to 0.07. The frequency of the vertical spring back mode increased slightly and the damping ratio is almost doubled at 0.31. The damping ratio of the pendulum mode decreased and is now considered marginally unstable. Lastly, the frequency of the longitudinal spring back mode almost doubled to 1.69 $\frac{rad}{sec}$ and its damping ratio increased from 0.38 to 0.90. Table 4 lists the eigenvalues of the multi-body modes with the baseline controller.

Of particular interest is to study the effect these multi-body modes have on the attitude disturbance rejection properties of each helicopter. Disturbance rejection performance can be

Table 4. Unique dynamic modes present in a dual lift pendant configuration with baseline controller

Mode Description	Eigenvalue	Frequency $\frac{rad}{sec}$	Damping
Helicopter Divergence	$0.017 \pm 0.80i$	0.80	-0.021
Lateral Spring Back	$-0.05 \pm 0.72i$	0.72	0.07
Longitudinal Spring Back	-1.521 ± 0.7286	1.69	0.90
Vertical Spring Back	$-0.40 \pm 1.24i$	1.3	0.31
Pendulum Mode	$0.004 \pm 1.5i$	1.5	-0.003

quantified by two metrics: disturbance rejection bandwidth (DRB) and disturbance rejection peak (DRP) (Ref. 26). DRB is a measure of the aircraft's ability to reject external disturbances and is defined to be the frequency at which the disturbance rejection frequency response is $-3dB$. DRP is a measure of overshoot for disturbance inputs and is determined by the peak magnitude of the disturbance response. For a dual lift system we shall define two DRP values. DRP_{DL} is defined to be the peak magnitude within the frequency range of the dual lift multi-body modes, 0.2 to $2 \frac{rad}{sec}$, and DRP_{HF} is the peak magnitude at high frequency (above $2 \frac{rad}{sec}$).

For the lateral (roll) axis, ADS-33E defines the maximum

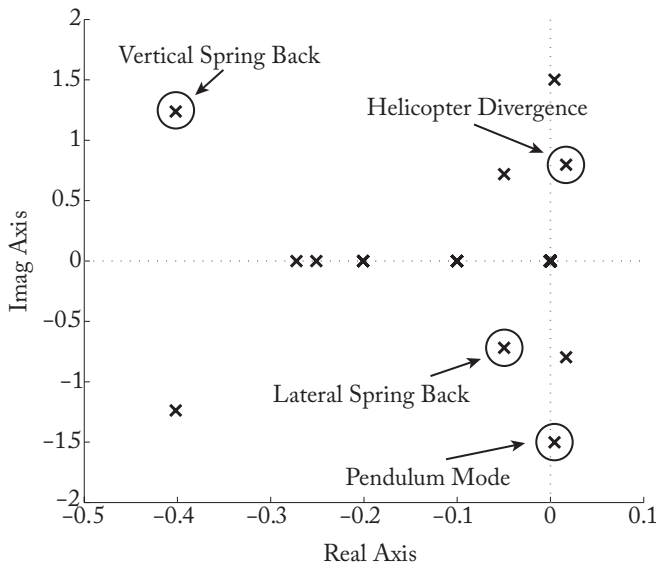


Fig. 18. Low frequency dual lift modes with baseline controller

allowable peak magnitude to be 5 dB (i.e. $DRP \leq 5dB$) and the minimum rejection bandwidth to be $0.9 \frac{rad}{sec}$ (i.e. $DRB \geq 0.9 \frac{rad}{sec}$). Figure 19 shows the roll disturbance rejection response of helicopter 1 (similar response seen for helicopter 2). The effects from the lateral spring back, helicopter divergence, and pendulum modes can be seen by the three distinct peaks present in the frequency response. As a result, the lateral spring back and divergence modes decrease the DRB of the system. With the baseline controller, the roll axis DRB is $0.62 \frac{rad}{sec}$, less than the ADS-33E requirement. In addition, the divergence and pendulum modes cause DRP_{DL} to be greater than the ADS-33E maximum of 5 dB, while DRP_{HF} meets the requirement.

For the longitudinal (pitch) axis, ADS-33E defines the maximum allowable peak magnitude to be 5 dB (i.e. $DRP \leq 5dB$) and the minimum rejection bandwidth to be $0.5 \frac{rad}{sec}$ (i.e. $DRB \geq 0.5 \frac{rad}{sec}$). Figure 20 shows the pitch attitude disturbance rejection response for helicopter 1 (similar response seen for helicopter 2). The helicopter divergence mode causes DRP_{DL} to be greater than the ADS-33E maximum of 5 dB, while both DRB and DRP_{HF} requirements are satisfied.

It is clear that a dual lift pendant system poses unique control challenges and that additional augmentation is needed in order to stabilize the system and improve its disturbance rejection properties.

Feedback Effects of Unique Dual Lift Parameters

To minimize alterations to the existing control laws and keep the design modular, a dual lift controller is added to the roll, pitch, and vertical inner-loops of each helicopter according to the block diagram of Figure 17. The same controller with the same gains are used for both aircraft. Due to the nature of the multi-body modes and the presence of a slung load, the

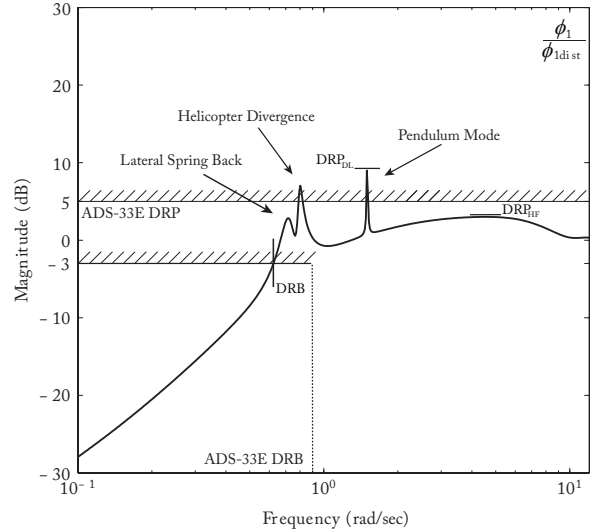


Fig. 19. Roll disturbance rejection response for helicopter 1 with baseline controller

feedback effects of the following variables for each helicopter were considered:

- ϕ, θ : Attitude
- p, q : Attitude rate
- v_z : Vertical velocity
- ϕ_c, θ_c : Roll/pitch cable angle
- $\dot{\phi}_c, \dot{\theta}_c$: Roll/pitch cable angle rate
- $\Delta y, \Delta x$: Lateral/longitudinal helicopter separation
- $\Delta \dot{y}, \Delta \dot{x}$: Lateral/longitudinal helicopter rate of closure

The unstable divergent mode observed in the baseline system was dominated by helicopter separation in the longitudinal axis, suggesting that longitudinal separation or longitudinal rate of closure feedback would help stabilize the system. Figure 21 shows a root locus of the system roots for increasing longitudinal helicopter rate of closure gain, $k_{\Delta \dot{x}}$. As $k_{\Delta \dot{x}}$ is increased, the helicopter divergent mode is stabilized at the expense of reducing the frequency and damping of the longitudinal spring back mode. Once stabilized, the divergent mode acts as another slow spring back type mode.

As a consequence of stabilizing and damping the divergent mode, the disturbance rejection properties also improve. The pitch DRP_{DL} is significantly reduced, but so is the DRB (Fig. 22). This decrease in DRB can be mitigated by increasing the pitch attitude gain (Fig. 23) at the expense of a larger DRP_{HF} , showing a clear trade-off between using rate of closure and attitude gain to improve disturbance rejection properties.

Cable angle and cable angle rate feedback was implemented in an attempt to provide additional load damping as

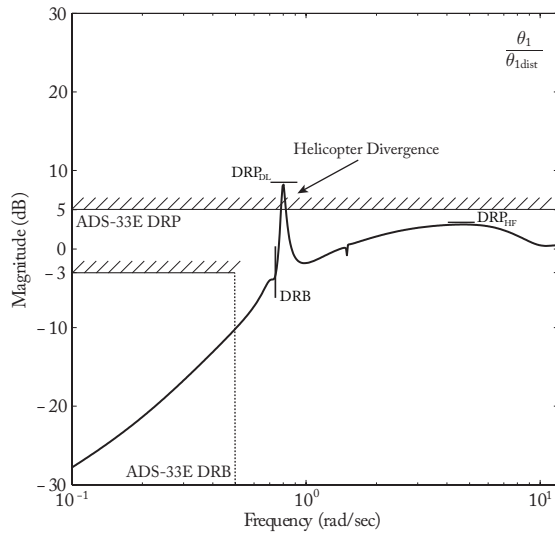


Fig. 20. Pitch disturbance rejection response for helicopter 1 with baseline controller

was done by Ivler, et al. in Reference 27 for a single lift system. Ivler showed that cable angle rate feedback provides damping to the load response at the cost of degraded handling qualities that is associated with a poor attitude response. Figure 24 shows the root locus of the dual lift system for roll cable angle rate feedback, k_{ϕ_c} . Similar to what is observed in a single lift system, roll cable angle rate feedback degrades each individual helicopter's lateral phugoid. However, unlike a single lift system, cable angle rate feedback does not provide significant load damping. This fact is due to the proximity of the pendulum mode to a transmission zero. A similar behavior is observed for pitch cable angle rate feedback. Therefore, traditional body relative cable angle rate feedback cannot be used to provide adequate load damping before destabilizing the lateral or longitudinal phugoids of each helicopter. Instead, a direct measure of the load swinging motion is needed.

In a dual lift system, it is possible to have changes in cable angle that does not correspond to a swinging load. For example, if both helicopters were to simultaneously fly in a circle around the load, the cable angles of each helicopter would be changing, however, the load would remain stationary as depicted in Figure 25. In order to capture the swinging motion of the load, a roll/pitch load-swing angle can be defined as

$$\phi_{sw_i} \triangleq \phi_{NS_i} - \phi_{ci} \quad \text{for } i = 1, 2 \quad (13)$$

$$\theta_{sw_i} \triangleq \theta_{NS_i} - \theta_{ci} \quad \text{for } i = 1, 2 \quad (14)$$

where ϕ_{NS} and θ_{NS} are cable angles for a no-swing, or hover trim, condition. Equivalently, this condition corresponds to the cable angles when the load lies on a vertical plane that contains the hook attachment points of each helicopter as is depicted in Figure 14.

Figure 26 shows the significant differences between the roll cable angle and load-swing angle frequency responses of helicopter 1, for a lateral input. The load-swing angle response exhibits a traditional lightly damped second order

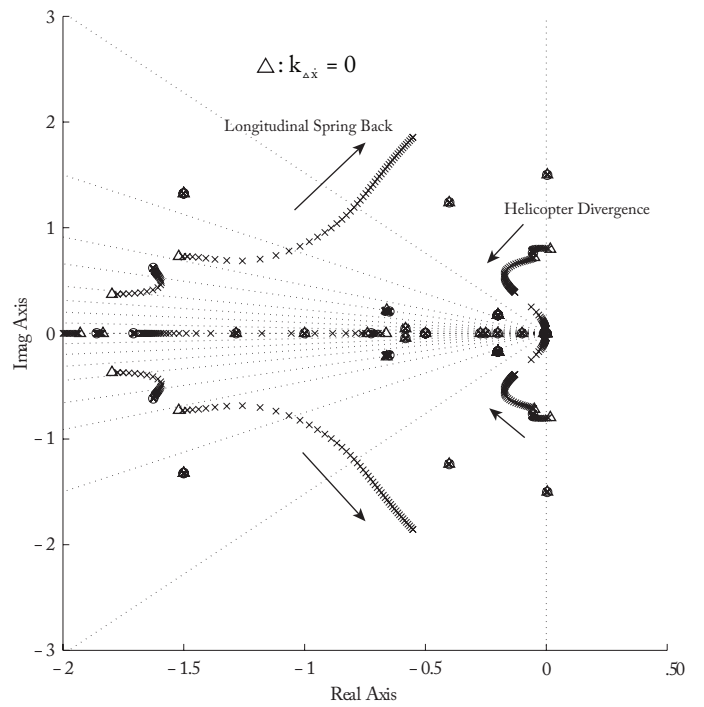


Fig. 21. Root locus of dual lift roots for increasing longitudinal helicopter rate of closure gain ($k_{\Delta \dot{x}}$)

shape. In turn, feeding back load-swing cable angle rate gives the desired effect of damping the load swinging motion (Fig. 25) and is used as a feedback measurement instead of traditional cable angle rates.

Multi-Objective Control Law Optimization

Based on the observed feedback effects, the final set of gains incorporated in the dual lift controller for each aircraft are:

- k_{ϕ}, k_{θ} : Attitude
- k_{v_z} : Vertical velocity
- $k_{\phi_{sw}}, k_{\theta_{sw}}$: Load-swing cable angles
- $k_{\dot{\phi}_{sw}}, k_{\dot{\theta}_{sw}}$: Load-swing cable angle rates
- $k_{\Delta y}, k_{\Delta x}$: Lateral/longitudinal helicopter separation
- $k_{\Delta \dot{y}}, k_{\Delta \dot{x}}$: Lateral/longitudinal helicopter rate of closure

The dual lift inner-loop controllers were optimized in CONDUIT[®] (Ref. 28) to meet a comprehensive set of stability and performance requirements listed in Table 5. The set of specifications aim to provide the best achievable performance while maintaining adequate stability and minimizing control activity.

A comparison of the key control system performance metrics for the baseline and optimized dual lift controllers is provided in Tables 6-7. All stability margins and crossover frequencies were calculated for open loop responses broken at

Table 5. CONDUIT[®] control system design specifications

Specification	Description	Axes
EigLoG1	Eigenvalues in left-half plane	Roll, Pitch, Heave
StbMgG2	Gain and phase margin (10% increase)	Roll, Pitch, Heave
NicMgG1	Nichols margin robust stability	Roll, Pitch, Heave
EigDpG1	Damping ratio	Roll, Pitch, Heave
ModFoG2	Command model agreement	Roll, Pitch, Heave
BnwAtH1	Pitch and roll bandwidth requirement	Roll, Pitch
CrsMnG2	Minimum crossover frequency	Roll, Pitch
DstBwG1	Disturbance rejection bandwidth	Roll, Pitch
DstLoG1	Disturbance rejection peak magnitude	Roll, Pitch, Heave
OlpOpG1	Open loop operating point rate limit saturation	Roll, Pitch, Heave
RMSAcG1	Acuator root mean square (RMS)	Roll, Pitch, Heave

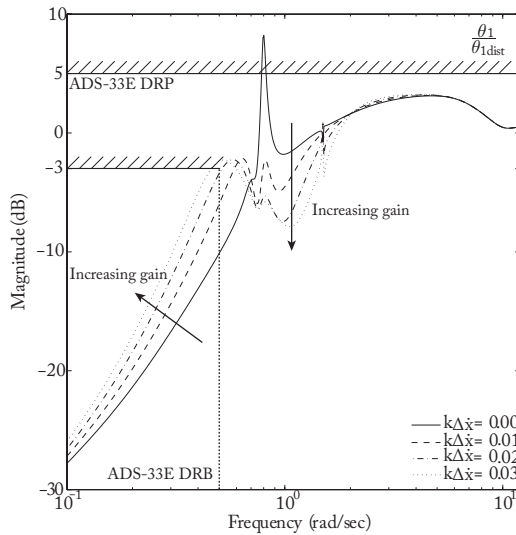


Fig. 22. Helicopter 1 pitch disturbance rejection response for increasing helicopter rate of closure gain, ($k_{\Delta \dot{x}}$)

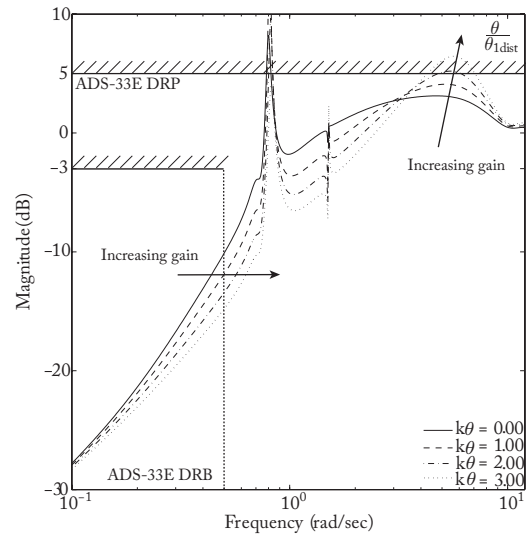


Fig. 23. Helicopter 1 pitch disturbance rejection response for increasing pitch attitude gain, (k_{θ})

the actuator. In addition, model following costs and phase bandwidth values were computed after replacing the pre-filters depicted in Figure 16 with new closed loop inverses of the feedback loops.

The optimized controller is able to stabilize the system and, for both axes, provide increased robustness by achieving a larger crossover frequency and a 10% increase in ADS-33E stability margin requirements. Enforcing a 10% increase in stability margin requirements provides additional latitude when designing velocity and position loops in the future.

Closed loop performance was improved as indicated by the smaller model following costs for the optimized system in both axes. Figure 28 shows a comparison between the desired closed loop pitch response, as defined by the command model, and the actual measured response. A close match and low model following cost results from a good transfer function fit of the closed loop inverse of the feedback loop. The ability to

achieve a good fit can be directly attributed to the well damped multi-body modes as indicated in Table 9. All spring back modes meet the required ADS-33E minimum damping ratio of 0.35 and a pendulum damping ratio of 0.11 was achieved. In contrast, the poor behavior of the multi-body modes in the baseline system result in a poor fit of the closed loop response and a higher model following cost, particularly in the roll axis.

Significant increase in disturbance rejection performance was also achieved. Figure 29 shows a comparison of the baseline and optimized roll disturbance rejection response. As compared to the baseline system, the DRB for the optimized system is a factor of three larger, mainly as a result of the dramatic decrease in DRP_{DL} . With clear improvements in DRB and DRP_{DL} , now both metrics, along with DRP_{HF} , meet ADS-33E requirements in both axes.

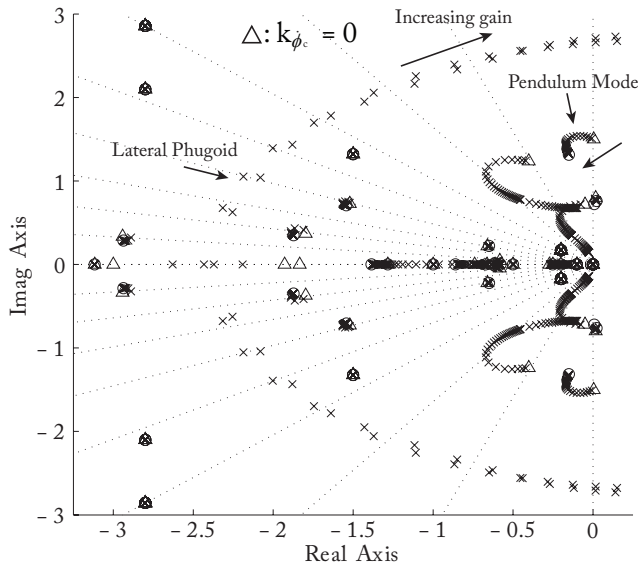


Fig. 24. Dual lift system roots for increasing roll cable angle gain, (k_{ϕ_c})

Table 6. Key Roll Axis Metrics

	Desired	Baseline	Optimized
ω_c [rad/sec]	≥ 2.80	2.36	2.84
PM [deg]	≥ 50.0	Unstable	50.1
GM [dB]	≥ 6.60	Unstable	9.73
ω_{BW} [rad/sec]	≥ 2.00	3.30	3.60
DRB [rad/sec]	≥ 0.90	0.62	1.79
DRP_{DL} [dB]	≤ 5.00	9.83	-0.15
DRP_{HF} [dB]	≤ 5.00	3.02	4.35
Model Following	≤ 50.0	81.8	6.00

The final gain values are listed in Table 8. Note that the objective of the dual lift inner-loop controller is not to regulate helicopter separation (as this is an outer-loop function), but to provide a robust attitude response for each helicopter in order to serve as a foundation for the outer-loop design. To reach this objective, only attitude and load-swing angle rate feedback with no lateral separation was needed in the lateral axis.

NONLINEAR SIMULATION

Two nonlinear simulations were conducted in the RIPTIDE[®] environment (Ref. 29), shown in Figure 30, to further evaluate the performance of the dual lift controller. In the first simulation, commands and disturbances are injected only into a single helicopter and the response of both aircraft are observed. In the second simulation both helicopters receive the same inputs.

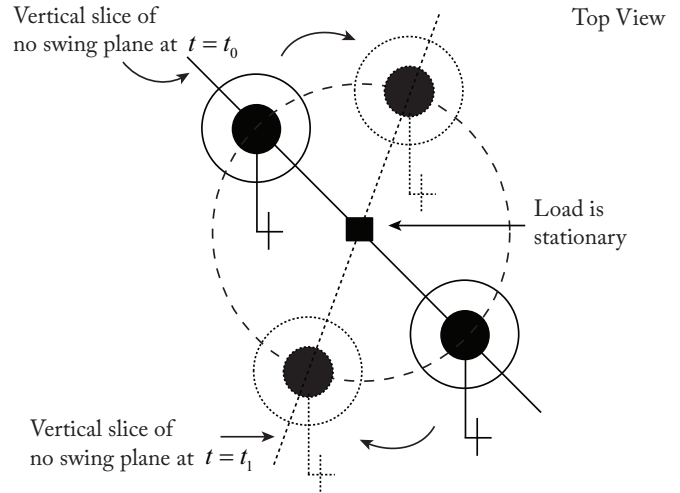


Fig. 25. Dual lift system flying in a circle around a stationary load, corresponding to changes in cable angle and no load swing

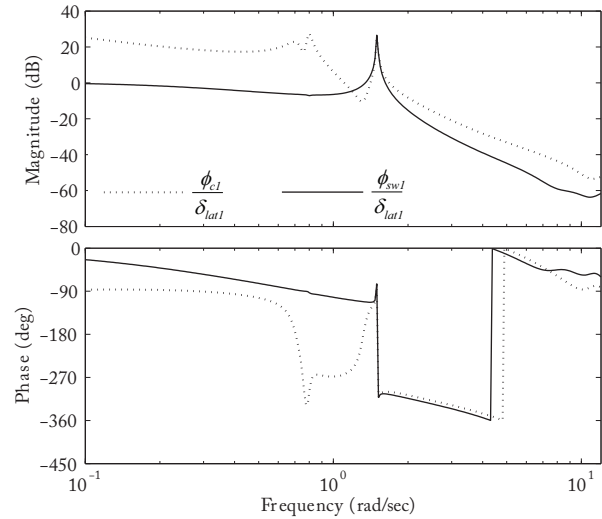


Fig. 26. Helicopter 1 roll cable angle (ϕ_{c1}) and load-swing angle (ϕ_{sw1}) frequency response for a lateral input

Table 7. Key Pitch Axis Metrics

	Desired	Baseline	Optimized
ω_c [rad/sec]	≥ 2.80	2.65	2.84
PM [deg]	≥ 50.0	Unstable	50.1
GM [dB]	≥ 6.60	Unstable	10.0
ω_{BW} [rad/sec]	≥ 2.00	2.66	2.82
DRB [rad/sec]	≥ 0.50	0.74	1.76
DRP_{DL} [dB]	≤ 5.00	8.19	0.78
DRP_{HF} [dB]	≤ 5.00	3.15	4.27
Model Following	≤ 50.0	24.1	17.5

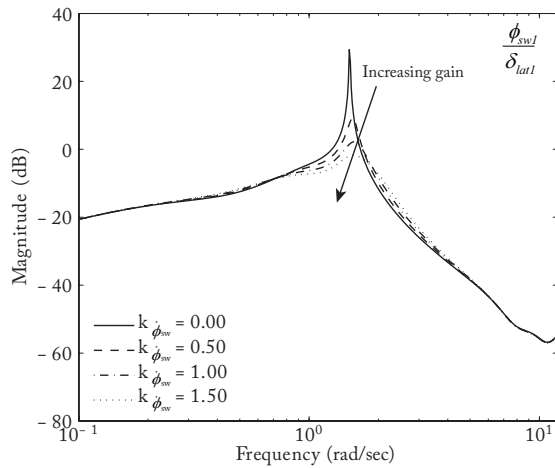


Fig. 27. Helicopter 1 load-swing angle (ϕ_{sw1}) frequency response for increasing load-swing angle rate gain, $k_{\dot{\phi}_{sw}}$

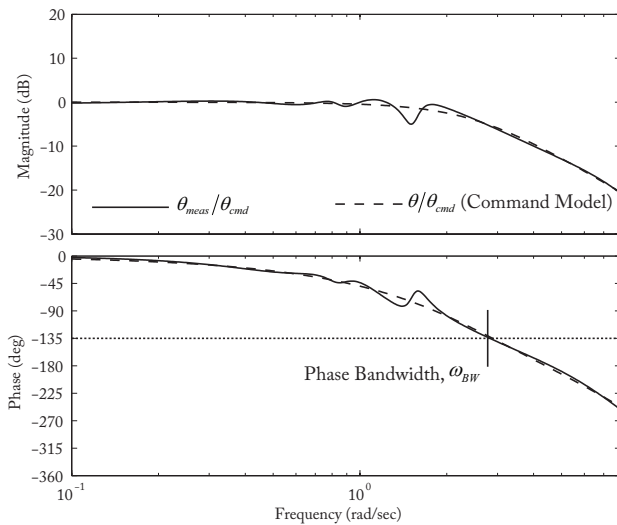


Fig. 28. Frequency response comparison between the pitch attitude command model and the measured response

Individual Helicopter Performance

To assess the closed loop response of an individual helicopter, a 5° pitch doublet was commanded into the lead aircraft (helicopter 1) while the trail aircraft (helicopter 2) received no input (i.e. commanded to maintain trim attitude). Figure 31 shows the resulting pitch attitude response of the lead helicopter. As was predicted by the low model following cost in the control law analysis, the closed loop response matches the commanded transient response closely with only small (0.5° peak-to-peak) decaying steady-state oscillations due to the swinging motion of the load. Figure 32 shows the attitude responses for both helicopters. The trail aircraft is able to regulate its response despite excitations in the load motion caused by the lead helicopter's movement.

The disturbance rejection properties were evaluated by commanding a 0.5 second, 10° pulse into the pitch attitude

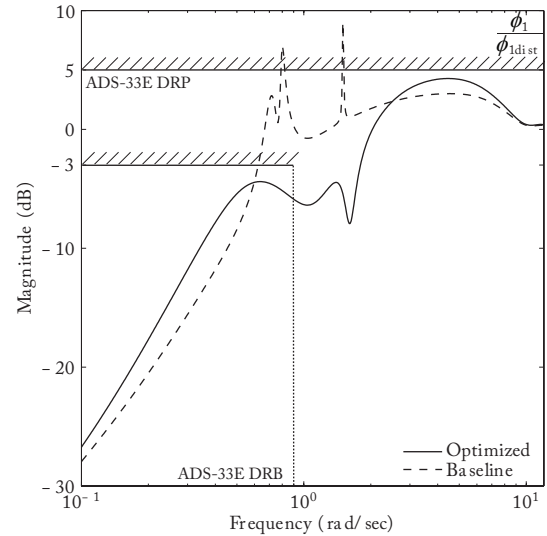


Fig. 29. Roll disturbance rejection response comparison between baseline and optimized controllers

Table 8. Optimized Controller Gain Values

Gain	Value
k_ϕ	0.99 [STU ^a /rad]
$k_{\phi_{sw}}$	0.00 [STU/rad]
$k_{\dot{\phi}_{sw}}$	0.92 [STU/rad]
$k_{\Delta y}$	0.00 [STU/ft]
$k_{\Delta \dot{y}}$	0.00 [STU-s/ft]
k_θ	0.76 [STU/rad]
$k_{\theta_{sw}}$	0.38 [STU/rad]
$k_{\dot{\theta}_{sw}}$	0.51 [STU/rad]
$k_{\Delta x}$	0.0076 [STU/ft]
$k_{\Delta \dot{x}}$	0.025 [STU-s/ft]
k_{vz}	0.82 [STU-s/ft]

^aSTU: Stick Units (-1 to 1)

Table 9. Dual Lift Multi-Body Modes With Optimized Controller

Mode Description	Eigenvalue	Frequency $\frac{rad}{sec}$	Damping
Helicopter Divergence	$-0.2 \pm 0.17i$	0.27	0.76
Lateral Spring Back	$-0.308 \pm 0.50i$	0.587	0.59
Longitudinal Spring Back	-0.37 ± 0.99	1.06	0.35
Vertical Spring Back	$-0.64 \pm 0.55i$	0.84	0.76
Pendulum Mode	$-0.18 \pm 1.57i$	1.58	0.11

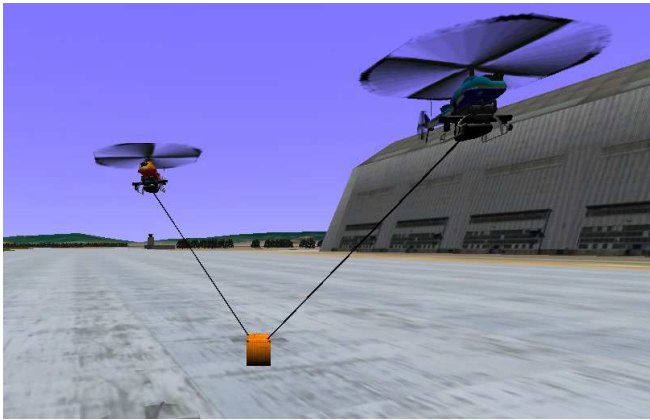


Fig. 30. Dual lift system in RIPTIDE® environment

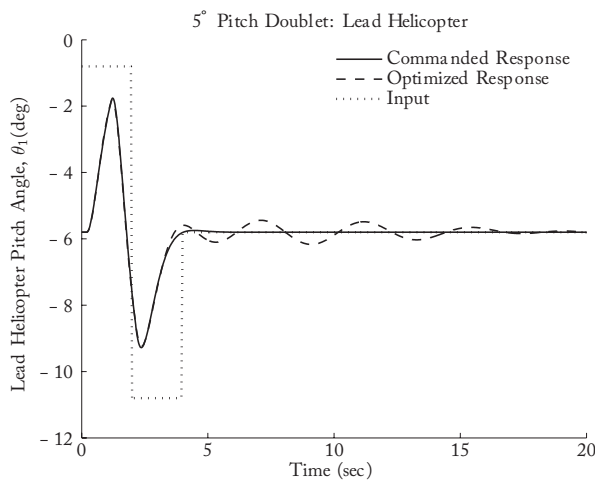


Fig. 31. Lead helicopter 5° pitch doublet

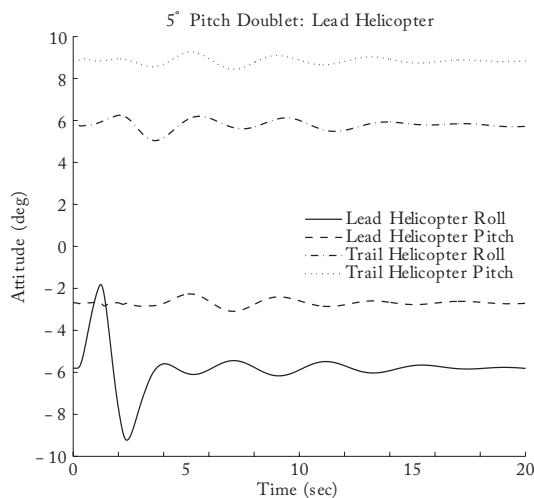


Fig. 32. Lead and trail attitude response for a lead helicopter 5° pitch doublet

measurement of only the lead aircraft. Figure 33 shows the pitch attitude response and the improved return to trim characteristics as predicted by the disturbance rejection metrics DRB and DRP_{HF} .

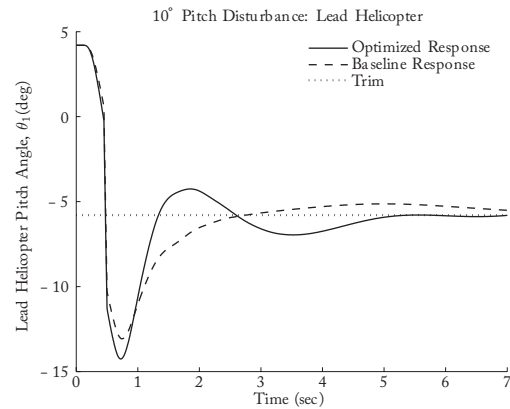


Fig. 33. Lead helicopter pitch response for a 10° disturbance in the lead helicopter only

Dual Lift System Performance

The closed loop performance of the dual lift system acting as a team was evaluated by commanding a 5° roll doublet to both aircraft simultaneously. Both aircraft attitude responses track their respective commands (Figs. 34 and 35) as was observed in the single helicopter input scenario, with some residual oscillations of about 4 seconds; corresponding to the dual lift pendulum mode frequency of $\omega = 1.5 \frac{rad}{sec}$ (See table 9).

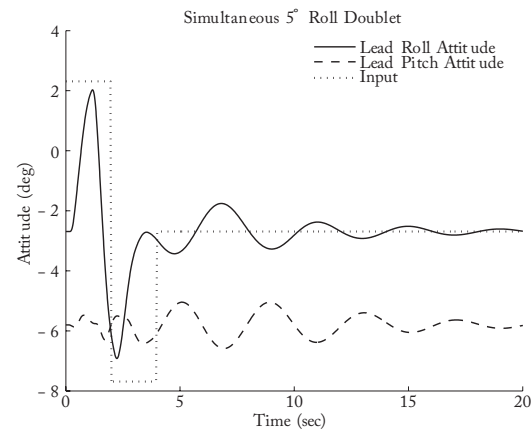


Fig. 34. Lead aircraft attitude response for a simultaneous 5° roll doublet

Lastly, to assess the system disturbance rejection characteristics, the payload was released from rest at a swing angle of 20° while both aircraft were commanded to maintain their respective trim attitudes. Figure 36 shows the lead helicopter's roll and pitch attitude response. An initial attitude

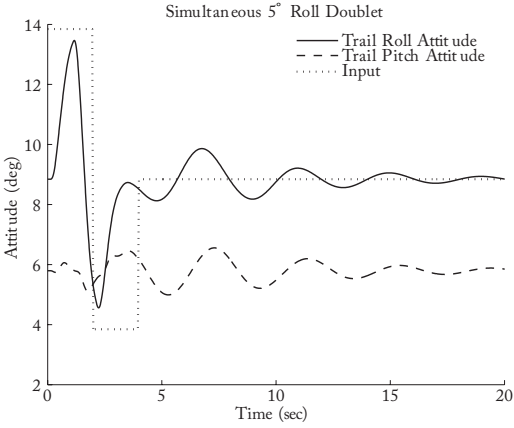


Fig. 35. Trail aircraft attitude response for a simultaneous 5° roll doublet

peak excursion of 5° is noted as the payload picks up speed and swings underneath the helicopters with amplitude and oscillations decaying over time. The trail helicopter's response is shown in Figure 37 showing similar behavior.

The overall system was designed to meet a comprehensive set of ADS-33E requirements and shows good closed loop and disturbance rejection performance. This inner-loop design provides a solid basis for outer-loop development.

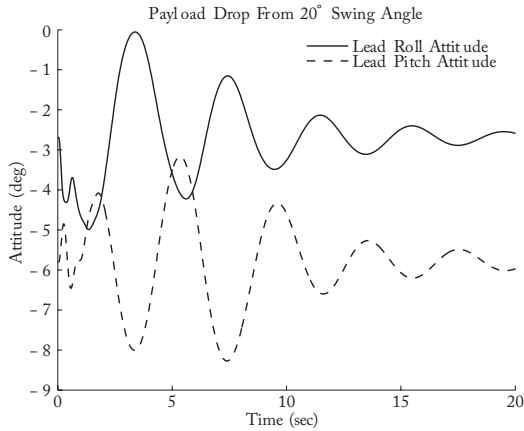


Fig. 36. Lead aircraft attitude response after payload is released from 20° swing angle

EFFECT OF FORMATION ANGLE ON DAMPING OF PENDULUM MODE

For most conventional helicopters, the roll axis moment of inertia is much less than that of the pitch axis. This difference in moment of inertia causes the lateral pendulum mode in a single lift system to inherently have a higher achievable damping ratio than the longitudinal mode. A standard UH-60 has roll and pitch moments of inertia of 4,659 slug-ft² and 38,512 slug-ft², respectively (Ref. 30). The damping ratios achieved by a load damping controller in Reference 31 for a UH-60

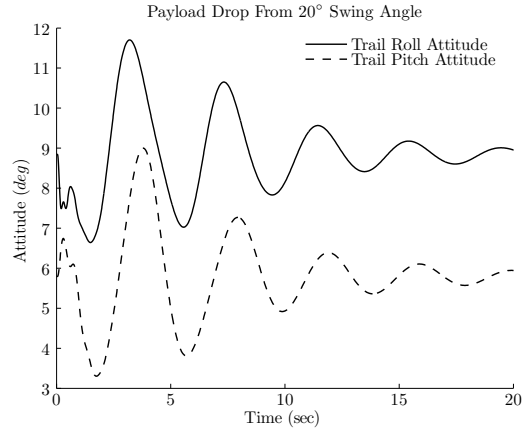


Fig. 37. Trail aircraft attitude response after payload is released from 20° swing angle

were $\zeta = 0.28$ and $\zeta = 0.25$ for the lateral and longitudinal pendulum modes, respectively. In a dual lift configuration, the formation angle determines the direction of load swing. For example, a formation angle of $\psi_f = 0$ degrees (side-by-side) restricts the load motion to be purely longitudinal, while a formation angle of $\psi_f = 90$ degrees (front-to-back) produces a purely lateral load swing. This behavior suggests that the achievable damping ratio of the dual lift pendulum mode might be a function of formation angle.

To study the effects of formation angle on the achievable damping ratio of the pendulum mode, the inner-loop dual lift controller was re-optimized for various formation angles. Figure 38 shows the obtained damping ratios as a function of formation angle. The achieved damping ratio for a purely lateral load swing ($\psi_f = 90$ degrees) is $\zeta = 0.155$ and $\zeta = 0.059$ for a longitudinal load swing ($\psi_f = 0$ degrees). This reduction in damping ratio is consistent with what is observed for a single lift system. In general, the dual lift pendulum mode damping ratio increases with formation angle and a coarse local maximum of $\zeta = 0.172$ is reached for a formation angle of $\psi_f = 45$ degrees, corresponding to the nominal configuration studied in this paper. In order to make a fair comparison the minimum crossover frequency requirement was reduced from 2.8 to $2.5 \frac{rad}{sec}$ to ensure that an optimized solution was reached for all formation angles. This explains the difference in achieved damping ratio for a formation angle $\psi_f = 45$ degrees as shown on Figure 38 and listed in Table 9.

The ability to control the direction of load swing with formation angle indirectly allows the dual lift system to vary the damping characteristics of the swinging load. This result suggests that a formation angle between $\psi_f = 45-90$ degrees would be preferable in hover to achieve best load damping and aid in maneuvers such as precise load placement. A formation angle of $\psi_f = 30-60$ degrees is common in formation cruise flight of two independent helicopters and also appears to be well suited for hover.

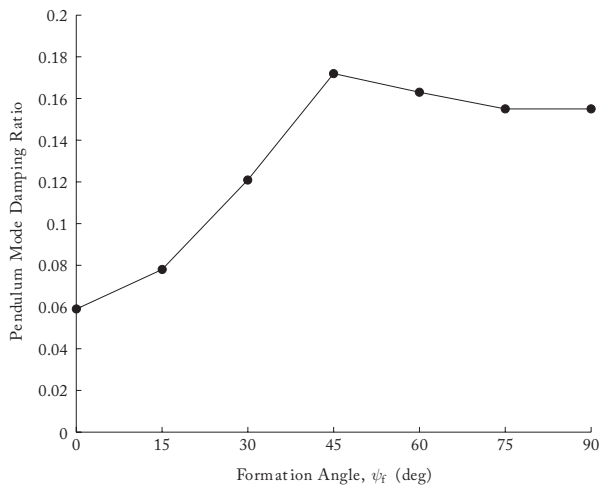


Fig. 38. Achievable pendulum mode damping ratio as a function of formation angle

CONCLUSIONS

A dual lift simulation model using R-MAX helicopters in a pendant configuration was developed and its numerical soundness verified. The unique stability characteristics of a pendant configuration were presented and a baseline inner-loop controller that does not account for dual lift dynamics was analyzed. The baseline controller was then augmented using standard fuselage and dual lift unique feedback parameters to achieve system stability and improved disturbance rejection properties. The following conclusions can be drawn from this study:

1. A representative dual lift pendant configuration that uses cable lengths and helicopter separation of two rotor diameters yields a 95% increase in lifting capability as compared to a single lift system.
2. Unique dual lift modes lie in a frequency range that affects the attitude response and should be considered when designing a multi-lift inner-loop controller.
3. Helicopter rate of closure feedback successfully stabilizes an unstable divergent mode and improves disturbance rejection properties.
4. In a dual lift pendant configuration, the payload only has a single degree of freedom and is constrained to move perpendicular to a local vertical plane containing the hook attachment points of both helicopters. Consequently, a cable angle that is relative to a no swing plane is used to characterize the swinging motion and improves damping of the payload.
5. A multi-objective parametric optimization approach proved successful to choose a set of feedback gains to meet a broad set of performance specifications for a complex dual lift multi-body system.

6. The achievable damping ratio of the dual lift pendulum mode is a function of formation angle. Highest damping is obtained for formation angles between $\psi_f = 45$ -90 degrees, suggesting these formation angles would be preferable in hover to achieve best load damping and aid in precision load placement.

REFERENCES

- [1] Meier, W. and Olson, J., "Efficient Sizing of a Cargo Rotorcraft," *AIAA Journal of Aircraft*, Vol. 25, (6), 1988.
- [2] Maciolek, J., "Feasibility Study for Multiple Helicopter Heavy Lift Systems," VERTOL Report R-136, prepared for Transportation Research and Engineering Command, Contract No. DA-44-177-TC-391, October 1957.
- [3] Meek Jr., T. and Chesley, G., "Twin Helicopter Lift System Study and Feasibility Demonstration," Sikorsky Engineering Report 64323, prepared for US Army Aviation Material Directorate, December 1970.
- [4] Korsak, K., Meenen, K., Meyers, D., and Piasecki, F., "Multi-Helicopter Heavy Lift System Feasibility Study," NAVAIR Contract No. N62269-71-C-0581, Report No. 39-X-11, February 1972.
- [5] Lewis, J. and Martin, C., "Models and Analysis for Twin-Lift Helicopter Systems," Proceedings of the American Control Conference, June 1983.
- [6] Curtiss, H. C. and Warburton, F. W., "Stability and Control of the Twin Lift," *Journal of the American Helicopter Society*, Vol. 30, (2), April 1985.
- [7] Cicolani, L. and Kanning, G., *General Equilibrium Characteristics of a Dual-Lift Helicopter System*, NASA TP 2615, July 1986.
- [8] Cicolani, L. and Kanning, G., *Equations of Motion of Slung-Load Systems, Including Multilift Systems*, NASA TP 3280, 1992.
- [9] Hess, R. and Tran, P., "Pilot/Vehicle Analysis of a Twin-Lift Helicopter Configuration in Hover," *AIAA Journal of Guidance, Navigation, and Control*, Vol. 11, (5), September-October 1988.
- [10] Prasad, J., Schrage, D., and Mittal, M., "Comparison of Nonlinear Controllers for Twin-Lift Configurations," AIAA Guidance, Navigation, and Control Conference, August 1989.
- [11] Menon, P. and Prasad, J., "Nonlinear Control of a Twin-Lift Helicopter Configuration," *Journal of Guidance, Control, and Dynamics*, Vol. 14, (6), November-December 1991.
- [12] Song, Y., Horn, J., Li, Q., and Langealaan, "Modeling, Simulation, and Non-Linear Control of a Rotorcraft Multi-Lift System," 69th Annual Forum of the American Helicopter Society, May 2013.

- [13] Bernard, M., Kondak, K., and Hommel, G., "Load transportation system based on autonomous small size helicopters," *The Aeronautical Journal*, Vol. 114, (1153), March 2010, pp. 191–198.
- [14] Takahashi, M., Whalley, M., Fletcher, J., Morales, E., Ott, C., Olmstead, M., Goerzen, C., and Schulein, G., "Development and Flight Testing of Flight Control Laws for Autonomous Operations Research on the RASCAL JUH-60A," 68th Annual Forum of the American Helicopter Society, May 2012.
- [15] Whalley, M., Takahashi, M., Fletcher, J., Morales, E., Ott, C., Olmstead, M., Goerzen, C., Schulein, G., Savage, J., Burns, H., and Conrad, B., "Flight Test Results for Autonomous Obstacle Field Navigation and Landing Site Selection on the RASCAL JUH-60A," 69th Annual Forum of the American Helicopter Society, May 2013.
- [16] Takahashi, M., Whalley, M., and Schulein, G., "Flight Control Law Design and Development for an Autonomous Rotorcraft," 64th Annual Forum of the American Helicopter Society, April-May 2008.
- [17] Mansur, M., Tischler, M., Bielefield, M., Bacon, J., Cheung, K., Berrios, M., and Rothman, K., "Full Flight Envelope Inner-Loop Control Law Development for the Unmanned KMAX," 67th Annual Forum of the American Helicopter Society, May 2011.
- [18] Cicolani, L., Kanning, G., and Synnestvedt, R., "Simulation of the Dynamics of Helicopter Slung Load Systems," *Journal of the American Helicopter Society*, Vol. 40, (4), October 1995.
- [19] Mitiguy, P., "Advanced Dynamics for Mechanical, Aerospace, and Biomechanical Engineers," Self published textbook, November 2006.
- [20] Cheng, R., Tischler, M., and Schulein, G., "R-MAX Helicopter State-Space Model Identification for Hover and Forward-Flight," *Journal of the American Helicopter Society*, Vol. 51, (2), April 2006.
- [21] Kane, T. and Levinson, D., "A Method for Testing Numerical Integrations of Equations of Motion of Mechanical Systems," *Journal of Applied Mechanics*, Vol. 55, September 1988.
- [22] Cicolani, L., "R-MAX Slung Load Linearized Equations of Motion For Identification," Internal Technical Note, July 2008.
- [23] Prasad, J., Mittal, M., and Schrage, D., "Control of a Twin Lift Helicopter System Using Nonlinear State Feedback," *Journal of the American Helicopter Society*, Vol. 36, (4), October 1991.
- [24] Raz, R. and Rosen, A., "Trim and Stability of a Twin-Lift System in Forward Flight," *Journal of the American Helicopter Society*, Vol. 50, (2), April 2005.
- [25] Anon., "Handling Qualities Requirements for Military Rotorcraft, ADS-33E-PRF," U.S. Army Aviation and Missile Command, March 2000.
- [26] Blanken, C., Tischler, M., Lusardi, J., and Ivler, C., "Aeronautical Design Standard - 33 (ADS-33)... Past, Present, and Future," Handling Qualities Specialists' Meeting, Feb 2014.
- [27] Ivler, C. M., Tischler, M. B., and Powell, J. D., "Cable Angle Feedback Control Systems to Improve Handling Qualities for Helicopters with Slung Loads," AIAA Guidance, Navigation, and Control Conference, August 2011.
- [28] Tischler, M., Ivler, C., Mansur, M., Cheung, K., Berger, T., and Berrios, M., "Handling-Qualities Optimization and Trade-offs in Rotorcraft Flight Control Design," AIAA 25th Aerospace Sciences Meeting, November 2008.
- [29] Mansur, M. H., Frye, M., Mettler, B., and Montegut, M., "Rapid Prototyping and Evaluation of Control System Designs for Manned and Unmanned Applications," 56th Annual Forum of the American Helicopter Society, May 2000.
- [30] Howlett, J., "UH-60 Black Hawk Engineering Simulation Program: Volume 1 - Mathematical Model," NASA Technical Report CR-166309, 1981.
- [31] Ivler, C. M., Powell, J. D., Tischler, M. B., Fletcher, J. W., and Ott, C., "Design and Flight Test of a Cable Angle/Rate Feedback Flight Control System for the RASCAL JUH-60 Helicopter," 68th Annual Forum of the American Helicopter Society, May 2012.